Available online at www.sciencedirect.com

ScienceDirect

Proceedings of the Combustion Institute 35 (2015) 1595–1602

Proceedings of the Combustion Institute

www.elsevier.com/locate/proci

Droplet/ligament modulation of local small-scale turbulence and scalar mixing in a dense fuel spray

J. Shinjo [a,b,*], J. Xia [b], A. Umemura [c]

[a] Institute of Aeronautical Technology, Japan Aerospace Exploration Agency, 7-44-1 Jindaiji-higashimachi, Chofu, Tokyo 182-8522, Japan

[b] Mechanical Engineering Subject Area, School of Engineering and Design, Brunel University, Uxbridge, Middlesex UB8 3PH, United Kingdom

[c] Department of Aerospace Engineering, Nagoya University, Furocho, Chikusa-ku, Nagoya 464-8603, Japan

Available online 10 July 2014

Abstract

In this study, the modulation of turbulence and scalar mixing by finite-size droplets/ligaments in a dense fuel spray is investigated using a DNS (Direct Numerical Simulation) dataset. Ejected from a spray nozzle with a high speed, a liquid-fuel jet deforms and the fuel spray is atomized into many ligaments and droplets. During these processes, the gas flow becomes turbulent due to droplet/ligament dynamics. At the same time, droplet evaporation and mixing with ambient air are affected by the small-scale gas turbulence. An understanding of the mixing characteristics in the dense spray zone is important for modeling spray combustion. In a region where the droplet number density is relatively low, a universal feature of isotropic turbulence was found, although the alignments of strain eigenvectors with vorticity and the mixture fraction gradient are slightly modulated by the presence of droplets, which is a characteristic of particle-laden flows. In gas-phase regions close to droplet surfaces, where the dissipation rate of turbulent kinetic energy is strongly increased, the alignments are more modulated, especially those of the scalar gradient with strain eigenvectors. This can also be seen in the topology similarity among energy dissipation, enstrophy and scalar dissipation in the near field of droplet/ligament surfaces. For the first time, it is found that droplets whose size is comparable to turbulence scales do affect the mixing characteristics in a realistic turbulent spray. This finding has shed new light upon the modeling of flow turbulence and scalar mixing in an evaporating and atomizing fuel spray.

Keywords: DNS; Spray; Turbulence modulation; Scalar mixing; Small-scale structures

1. Introduction

Liquid-fuel atomization, evaporation, mixing and combustion closely interact with turbulence in spray combustion. The physics is very complex

* Corresponding author at: Mechanical Engineering Subject Area, School of Engineering and Design, Brunel University, Uxbridge, Middlesex UB8 3PH, United Kingdom. Fax: +44 1895 256 392.

E-mail address: Junji.Shinjo@brunel.ac.uk (J. Shinjo).

http://dx.doi.org/10.1016/j.proci.2014.06.088

since there is a wide range of temporal and spatial scales in an atomizing spray [1–6]. Droplets/ligaments are generated by primary atomization in the near-nozzle region, and the droplet size and distribution subsequently impose a significant impact on the downstream spray dynamics.

In the downstream dilute spray region, the turbulence scale is in general much larger than the droplet scale. While in the dense spray region near the injection nozzle, the turbulence scale is comparable to the droplet scale. For combustion, mixing of fuel/oxidizer is critical. Scalar mixing is strongly affected by small-scale turbulence structures [7–23]. Therefore, when the droplet/ligament size is comparable to the turbulence scale, it is expected that droplets/ligaments would change the small-scale structures, hence mixing. Despite its determining role in the entire spray combustion, droplet/ligament effects on turbulence and scalar mixing in a dense atomizing fuel spray have not been fully understood yet and will be the main objective of the present study.

In turbulent single-phase flows [7–14], correlations between turbulence structures and scalar mixing have been investigated. Abe et al. [14] conducted a DNS study in a heated channel to investigate scalar mixing. At the wall, small-scale structures are dominant due to high strain rates, and are different from those of isotropic turbulence. The small-scale topologies of the vorticity, energy dissipation and scalar dissipation rate become strongly correlated near the wall. Away from the wall, the correlations become weaker and the structures appear more similar to those of isotropic turbulence.

For turbulent multiphase flows, turbulence modulation by liquid droplets or solid particles has been of considerable interest [15–19]. In early studies [15–17], the particle size was much smaller than the turbulence scale, i.e. point particles. Particles, even at a low number density, modify the vorticity dynamics and turbulence production/dissipation rate by the drag force, and the turbulent mass and heat transport [15,16]. The alignments between the vorticity vector and strain eigenvectors are changed as a result of increased dissipation by the particles. Reacting flows laden with point-droplets were investigated by large-eddy simulation [17]. The turbulence modulation was induced by droplets (and heat release) due to the change of the alignments between the strain eigenvectors and the vorticity and also the scalar gradient. The effects of particles, whose size is comparable to the Kolmogorov or Taylor scales, on turbulence are also of interest recently [18,19]. The strain-rate eigenvalue modification was also observed for finite-size particles. In the near field of particles, the increased dissipation rate of turbulent kinetic energy due to the non-slip particle interface can be observed. In most of the studies above, the particles were solid and spherical. In this study, turbulent energy dissipation and heat/mass transport at the surface of deformable droplets/ligaments in a spray configuration are additional physical phenomena.

For simple configurations such as a single droplet or a droplet array in a gas flow, the flow-droplet interaction has been investigated extensively on turbulence, evaporation and combustion modes [20–23]. Although simple configurations are useful to improve our understanding, actual turbulent flow fields in a spray are more complicated. Since a dense liquid spray contains many droplets and ligaments, whose size is comparable to the turbulence scale, and the liquid–gas relative velocity is high, it is expected that turbulence modulation will occur. Formation of wake and vortex shedding by droplets/ligaments will change the production and dissipation of the gas-phase turbulence. This phenomenon can alter flow structures and fuel/oxidizer mixing, and thus impact the combustion characteristics in the downstream dilute spray region. Therefore, it is important to investigate the turbulent mixing of the gas phase with finite-size droplets in a fuel spray to properly model spray dynamics and combustion.

In this study, to elucidate the turbulent mixing characteristics in the dense spray region, the DNS dataset of the primary atomization of a liquid fuel jet is utilized. Since the droplet distribution is non-uniform due to atomization [3,4], the turbulence and mixing characteristics in regions with distinct droplet number densities are investigated. To the best of our knowledge, this is the first study on turbulence and scalar mixing in a dense fuel spray.

2. DNS of an evaporating and atomizing fuel spray [6]

The liquid fuel *n*-heptane is injected from a round nozzle of diameter $D_N = 0.1$ mm into hot quiescent air (900 K, 30 atm) at a high speed (100 m/s). The bulk liquid Weber number ($We = \rho_l U_l^2 a/\sigma$) is 14,100 and the bulk liquid Reynolds number ($Re = \rho_l U_l a/\mu_l$) is 1477, where $a = D_N/2$, ρ denotes density, U the injection velocity, σ the surface tension coefficient, μ viscosity and the subscript l denotes liquid. Slip velocity still exists between the liquid and gas phases, with the estimation of the Stokes number around 20 ($St = \rho_l D_{32}^2 U_s/18\mu_g L$, where D_{32} is the Sauter mean droplet diameter, U_s the slip velocity, L the characteristic flow length and the subscript g stands for gas) [6]. The droplet size is $D_{32}/\eta = 4.3$, where η is the Kolmogorov scale.

The governing equations for mass, velocity, temperature, interface shape and species mass fractions of C_7H_{16}, O_2, CO_2, H_2O, and N_2 are solved [6]. The global one-step reaction model by Westbrook is used [6]. The reaction heat release

is negligible in the dense spray region. (The temperature rise is below 1 K within the simulation period.) Therefore, both temperature and mixture fraction are nearly passive scalars, and the current results can be compared with those of Abe et al. [14] where the temperature is a passive scalar. The Lewis number is assumed to be unity. The evaporation rate is formulated by the equilibrium vapor pressure model and given by the jump condition at the interface [24]. The mixture fraction z is $z = (sY_F - Y_O + Y_{O,0})/(sY_{F,0} + Y_{O,0})$ with $s = \nu_O W_O/\nu_F W_F$. ν_i is the stoichiometric coefficient and W_i molecular weight. The subscript F denotes fuel, O oxidizer, and 0 the inlet condition for the fuel or oxidizer. $z = 1$ for the fuel stream and $z = 0$ for the air stream. The stoichiometric mixture fraction is $z_{st} = 0.062$.

Liquid–gas interfaces are captured by the level-set method and surface tension is formulated by the CSF (Continuum Surface Force) method. The advection term is solved by the CIP (Cubic Interpolated Pseudo-particle) method. The computational domain size is $5.5 \times 4.5 \times 4.5$ in D_N. The grid system is fixed on the jet head, which is $20D_N$ away from the injection nozzle [6]. The grid resolution is 0.35 μm, and the total number of grid points is 2.2 billion. Grid resolution tests have been done in our previous research on primary atomization and spray evaporation [3–6]. For cold-flow cases [3], where finer resolution is generally needed to capture smaller vortex structures due to a lower gas kinematic viscosity (thus a higher Reynolds number), the current resolution was sufficient. Additionally, several evaporating droplet cases at similar droplet Reynolds numbers have been tested to obtain satisfactory results of evaporation at droplet/ligament surface [6].

3. Results and discussion

Hereafter, an upper-case letter denotes the mean of a variable and a lower-case letter its fluctuation. For example, $u_{inst} = \bar{u} + u = U + u$, where *inst* stands for "instantaneous" and the bar denotes a mean value. In the present study, the time period for averaging to obtain a mean value is $\Delta\hat{t} = 1.5$, which is non-dimensionalized by D_N/U_l. x,y,z are also denoted by the subscripts 1,2,3, respectively, and the velocity components are u,v,w or u_1,u_2,u_3. $\partial a/\partial x_i$ is abbreviated as $a_{,i}$. The Einstein notation applies in $a_i b_i$, i.e. $a_i b_i = a_1 b_1 + a_2 b_2 + a_3 b_3$.

3.1. Overall flow field

Figure 1a shows the instantaneous shape of the liquid fuel jet head and gas-phase eddies visualized by the second invariant of the velocity gradient tensor (Q-value) [4,6]. At this time, the liquid jet head is $20D_N$ away from the nozzle. It is deformed like an umbrella due to the impact on the ambient air. At the head edge, the gas flow separates and large-scale vortex shedding occurs. A large recirculation zone is formed behind the jet head, where a significant amount of droplets/ligaments is detached from the liquid head edge and fine eddies are generated [6]. Jets or shear layers develop self-similarly in both the near-nozzle and downstream regions [25,26]. For the spray shown in Fig. 1, the recirculation zone develops self-similarly [4]. This is confirmed by the streamwise velocity profiles in the recirculation zone and the size development of the recirculation zone during the calculation time period (not shown).

Figure 2 shows the mean strain rate $S_{ij} = (1/2)(U_{i,j} + U_{j,i})$ in the recirculation zone, which is covered by the dashed rectangle in Fig. 1b. High shear is observed at the spray-jet head edge in the solid circle, where the gas flow separates and vortex shedding occurs. Much lower shear is observed on the periphery of the recirculation zone in the dashed ellipse, and the lowest near the liquid core in the dotted ellipse. It is expected that the flow field becomes closer to isotropic turbulence when the mean shear is low.

At $\hat{t} = 0$, the gas-phase flow is quiescent. All the gas kinetic energy is supplied from the injected liquid [3]. Part of the energy is initially used to form the umbrella-like jet head, and the residual is supplied to the gas flow through high-shear regions to form the recirculation zone behind the jet head, which is a large-scale energy-containing region of the gas flow. The gas-phase kinetic energy is about 7% of the total energy of the injected liquid at the time of Fig. 1 [3]. At this stage, most of the energy is being transferred to the gas through the atomized droplets and ligaments. The turbulent Reynolds number is defined as $Re_\lambda = u'\lambda/\nu$ where $\lambda = \left(\overline{u^2}/\overline{u_{,1}^2}\right)^{1/2}$ is the Taylor microscale in the axial direction, u' the root-mean-square (rms) of the axial velocity fluctuation and ν the kinematic viscosity. It is almost the same ($Re_\lambda \sim 60$) during the current simulation period.

3.2. Unsteady flow dynamics around droplets and ligaments

Before presenting turbulence statistics, unsteady mixing dynamics around droplet wake regions is investigated due to its close relation to turbulence generation and small-scale turbulent scalar mixing. Fig. 3 shows an example of vortex shedding in the recirculation edge region where the local droplet number density is high ($\sim 3 \times 10^{14}\,\mathrm{m}^{-3}$). The gas phase flows from the lower-right region to the upper left, as indicated by the streamlines in Fig. 3c. Figure 3a shows a 3D view of liquid structures superimposed on a

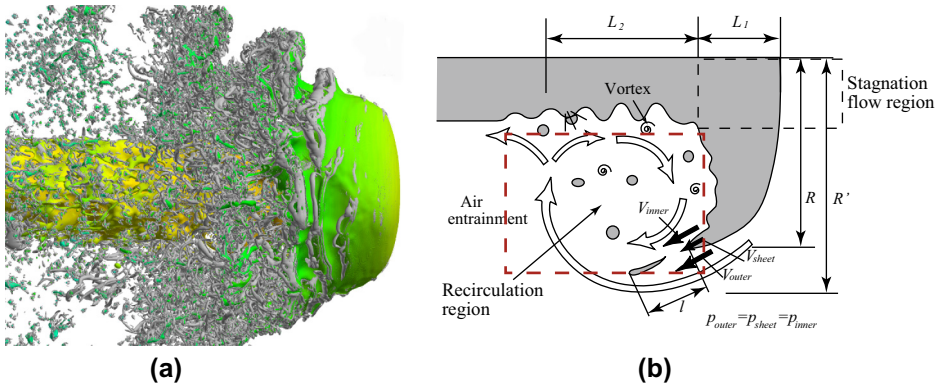

Fig. 1. Overall liquid structures and gas-phase eddies.

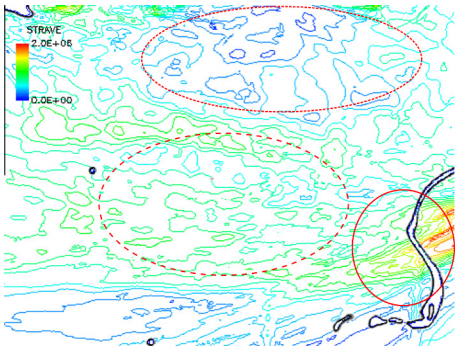

Fig. 2. Mean strain rate S (s^{-1}). The instantaneous liquid shape is shown for reference.

plane view of the fuel mass fraction Y_F. The red arrow indicates a front ligament in the gas flow. Several droplets and ligaments exist behind this ligament. Figure 3b and c present Y_F at a later time when mixing is more developed. The Reynolds number of the front ligament is 230, which is larger than the critical Reynolds number for the Karman vortex shedding over a cylinder in a uniform flow ($Re_c \sim 50$ [27,28]). Therefore, the Karman vortex shedding occurs as seen in Fig. 3. The observed Strouhal number is 0.23. The kinematics of fuel gas pockets is strongly affected by these vortices. Evaporated fuel gas pockets from each droplet/ligament can easily interact with each other and form a larger cluster of fuel vapor in a short time. Here, the local inter-droplet distance L is $L/D_{32} \leqslant 5$. Qualitatively, this clustering phenomenon is similarly observed for droplet arrays with a small inter-droplet distance [22].

In a region where the local droplet number density is smaller (the far left side in Fig. 1), the

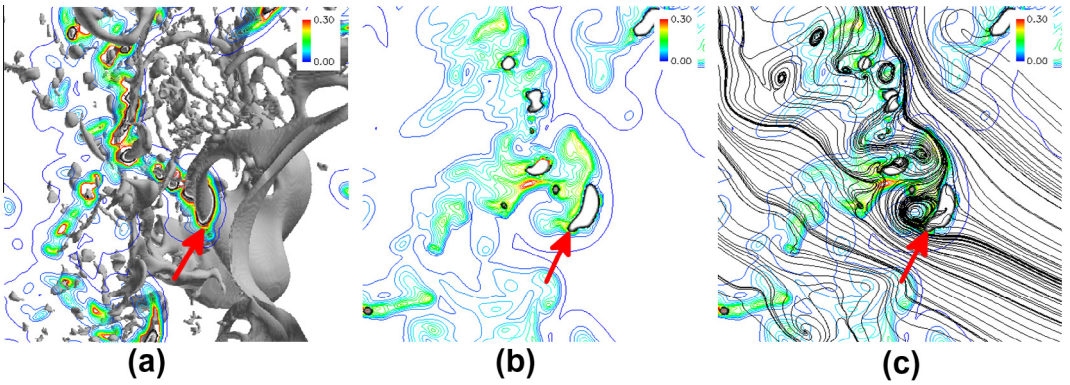

Fig. 3. Unsteady flow dynamics around droplets/ligaments. At an earlier time $\hat{t} = +0.32$, evaporation is strong and fuel-vapor/air mixing starts; at a later time $\hat{t} = +0.42$, evaporation becomes weaker, and fuel vapor and air are better mixed. (a) Liquid structures and Y_F at $\hat{t} = +0.32$, (b) Y_F at $\hat{t} = +0.42$, (c) streamlines and Y_F at $\hat{t} = +0.42$.

droplet Reynolds number is lower ($Re_d < 30$). On the other hand, the velocity fluctuation of the gas flow is typically much larger. Here, vortex shedding from each droplet is also observed because the incoming velocity-fluctuation is large ($u'/U \sim 0.3$). Even for low Re_d, the Karman vortex shedding occurs when the gas-flow velocity-fluctuation is large [27,28]. The inter-droplet distance is $L/D_{32} \geqslant 8$. Each fuel gas pocket is affected by these vortices, but is typically isolated (not shown).

The above unsteady vortex shedding is the source of turbulence generation. The vortices are convected away from the mean wake region. Thus, the gas flow is turbulent even in the recirculation zone where the droplet number density is low (shown later). In the high number-density region, the mutual interaction among wakes makes the wake survival slightly longer. In both regions, vortex shedding by droplets/ligaments alters the local flow structures and mixing at the droplet scale, and thus at the turbulence scale. A rough estimation of the droplet evaporation Damköhler number Da_v using the classical formulation [23] is $Da_v \sim$O(0.01–0.1), which suggests a slight increase in evaporation due to turbulent eddies around droplets in the dense spray region [6]. In the downstream dilute spray region where the droplet Stokes number reduces, the wake characteristics are different and therefore the turbulence and mixing characteristics are different accordingly.

3.3. Turbulence structures and mixing characteristics

The turbulent production terms for $\overline{\omega_i\omega_i}$ and $\overline{z_{,i}z_{,i}}$ are $\overline{\omega_i\omega_j s_{ij}}$ and $-\overline{z_{,i}z_{,j}s_{ij}}$, respectively, where $s_{ij} = (1/2)(u_{i,j} + u_{j,i})$ is the fluctuating strain tensor. The alignments between the vorticity ω_i, the scalar gradient $z_{,i}$ and the principal rate of s_{ij} are important to determine the variation of the turbulent production terms [7–14]. Since s_{ij} is symmetric, the eigenvalues a, b, c are real and satisfy $a \geqslant b \geqslant c$ $(a \geqslant 0 \geqslant c)$ and $a + b + c = 0$. Hereafter, the eigenvectors are denoted as **a**, **b**, **c** for the eigenvalues of a, b, c, respectively.

Figure 4 shows the probability density functions (PDFs) of the cosine of the angle of the alignment between the eigenvectors and ω_i or $z_{,i}$ in an area far away from the major liquid structures (encircled by the dashed line in Fig. 2). $\cos\theta = \pm 1$ means strong alignment and $\cos\theta = 0$ no alignment. The mean shear normalized by the Kolmogorov velocity and length scales is $S^* < 0.1$, thus the mean strain effect is not dominant here. The circles and triangles in Fig. 4 are from the literature for isotropic turbulence [10], isotropic turbulence with a mean scalar gradient [11] and a turbulent channel flow with wall heat transfer [14]. Known as a universal feature of isotropic turbulence, ω_i and $z_{,i}$ align with the intermediate (b) and compressive (c) strain rates, respectively [10,11]. In [14], this trend was also observed in the far-wall region out of the boundary layer. The current results show the same trend. Turbulent eddy generation is strongly correlated with wake formation due to droplets/ligaments. When the eddies are convected to the central region of the recirculation zone where the droplet number density is low, the flow there exhibits similar characteristics to gas-phase isotropic turbulence. The PDF of the normalized intermediate eigenvalue $b^* = \sqrt{6}b/\sqrt{a^2 + b^2 + c^2}$ is plotted in Fig. 5. It shows that b^* is mostly positive and thus extensional. This was also observed in [11,12,17]. The vorticity can have both sheet-like and tube-like structures [9]. When a vortex sheet wraps up, a tube-like structure is formed. By the alignment with b^*, it will be stretched and become longer along its axis with increased rotational motion [14,17] (see the sketch in Fig. 4a). This

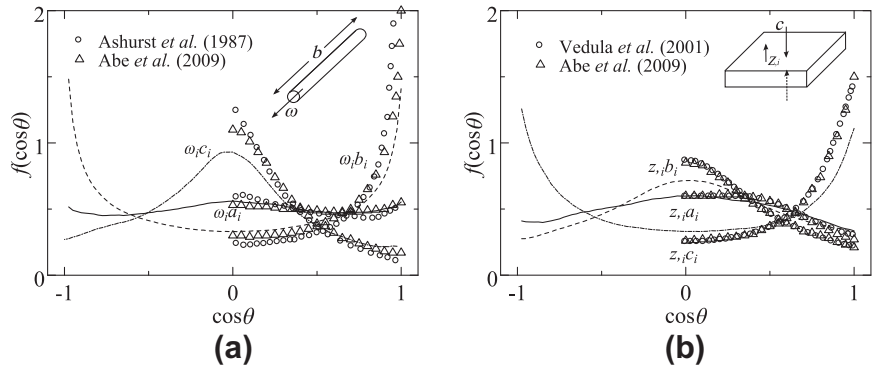

Fig. 4. PDFs of the alignment angles between the principal strain rates and (a) ω_i, (b) $z_{,i}$ in a region where the mean shear and droplet number density are low. (a) Vorticity (b) scalar gradient.

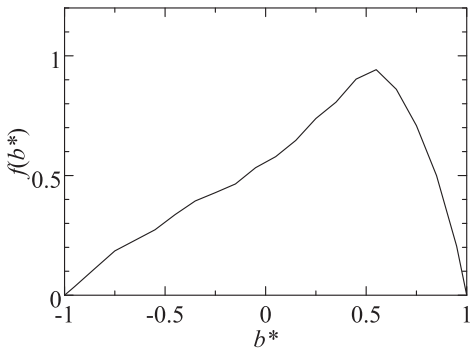

Fig. 5. PDF of the normalized intermediate eigenvalue b^*.

sheet-to-tube process indicates a process of energy cascade from large scales to small scales [9,17]. The alignment of $z_{,i}$ with the compressive strain rate c means that $z_{,i}$ is sheet-like (see the sketch in Fig. 4b). The $z_{,i}$ sheets will wrap tube-like structures of vorticity [9]. Therefore, it has been shown that turbulence structures similar to those in canonical turbulent flows [7–14] also develop in the dense fuel spray in a region away from the major liquid structures.

In Fig. 4, some discrepancies between the statistics of the dense fuel spray and those of isotropic turbulence can be observed. The alignment of ω_i with **b** is reduced, while that with **c** is increased. For $z_{,i}$, the alignment with **c** is reduced, while that with **b** is increased. (Reduced alignment can be indicated by reduced PDF near $\cos\theta = \pm 1$ and increased PDF near $\cos\theta = 0$; similarly for increased alignment.) The same modulation is similarly observed in flows laden with point particles/droplets [15–17] and with finite-size particles [18,19]. Particles increase the local velocity gradients, thus the strain rate s_{ij} and energy dissipation $\varepsilon = 2\nu s_{ij}s_{ij}$ [15–20]. Even if the particle number density is low, the strain rate eigenvalues are increased ($s_{ij}s_{ij} = a^2 + b^2 + c^2$) and the alignments are affected. Figure 6 shows an instantaneous snapshot of the energy dissipation rate, in which droplets are edged by black lines. The existence of droplets increases the local dissipation.

In near-droplet regions ($L/D_{32} < 1/4$), the alignments are changed by stronger local dissipation due to droplets/ligaments boundary layer formation. As shown in Fig. 7, ω_i still aligns with the intermediate (b) strain rate. However, the alignments of $z_{,i}$ with the compressive (c) and extensional (a) strain rates switch to an orientation angle of about 45° ($\cos\theta = \pm 0.7$). Both trends of the alignment of ω_i and $z_{,i}$ with the principal strain rates are the same as those in the near-wall region of channel flow turbulence (Fig. 4 of [14]). This implies that the droplet surface acts like a wall, makes the local flow non-isotropic and changes the local mixing characteristics.

To see this further, topologies of energy dissipation ε, enstrophy $\omega_i\omega_i$ and scalar dissipation $Dz_{,i}z_{,i}$ are investigated. D is the mass diffusion coefficient. Figure 8 shows instantaneous snapshots. The positive Q-value is superimposed using solid lines to identify vortex structures. Ligaments and droplets exist mostly in the lower right region and there are few liquid structures in the central region. For isotropic turbulence, the energy dissipation and enstrophy are alike because $\overline{\varepsilon} = \nu\overline{\omega_i\omega_i}$. The structures of ε and $\omega_i\omega_i$ are similar in the central region, as shown in Fig. 8a and b. As indicated by the red arrows, the structures of ε, $\omega_i\omega_i$ and $Dz_{,i}z_{,i}$ wrap a vortex (indicated by the blue arrow) with some phase-angle difference. This is characteristic to isotropic turbulence. Meanwhile, near the liquid surface in the lower right region, all the structures become similar. This was similarly observed in [14]. The physical reason is that the strong velocity and scalar gradients near the surface lead to $\omega_i\omega_i \sim (\partial u/\partial x_n)^2$ and $Dz_{,i}z_{,i} \sim D(\partial z/\partial x_n)^2$ where x_n is the wall normal direction.

The quantified topology correlations in the far- and near-surface regions are shown in Fig. 9 using joint PDFs. The joint PDFs are obtained by one realization data of Fig. 8. The axes represent the values normalized by the mean of samples in each region. In the far-surface region, the correlations are weak between the scalar dissipation and enstrophy (Fig. 9b) and between the scalar dissipation and energy dissipation (Fig. 9c). Meanwhile in the near-surface region, the corresponding correlations (Fig. 9e and Fig. 9f) are relatively stronger.

The PDF shapes in both regions are similar to those in [13,14]. The no-slip droplet surfaces form layers of velocity, temperature and scalar gradients, hence changing the local flow topology. Since the mixing time scale is linked to the scalar dissipation rate, the mixing characteristics near the surfaces are also changed. It is expected that if the Reynolds, Prandtl and Schmidt numbers are similar to the present study, this effect is generic in multiphase turbulent flows where the wall modulation exists.

4. Concluding remarks

The turbulence and mixing characteristics in a dense fuel spray, which is critical to combustion, have been investigated using DNS data. In the dense spray zone, turbulence is generated by the atomization dynamics, meanwhile droplets/ligaments modulate the small-scale turbulence

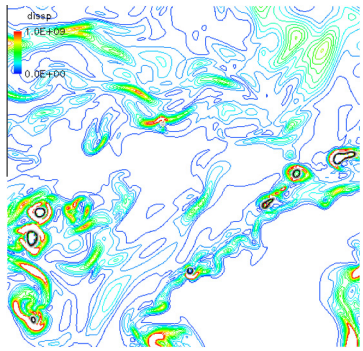

Fig. 6. Increased energy dissipation ($m^2\,s^{-3}$) around droplets.

characteristics, hence mixing. In most of the gas-phase regions except for near-surface regions, the alignments of the vorticity and scalar gradient with the principal strain rate eigenvectors show similar trends to those of isotropic turbulence. This indicates the turbulent energy cascade from large scales to small scales. The observed small discrepancies of the alignments between the dense fuel spray and isotropic turbulence are due to the increased gas-phase energy dissipation by the existence of droplets, which is a characteristic of particle-laden turbulent flows. In regions close to droplets, the alignments are different due to increased local energy dissipation by droplets, which affects the local small-scale fuel/air mixing. The effects of finite-size droplets, namely wake formation, vortex shedding and near-wall gradients generation, on turbulence and mixing in a realistic dense fuel spray have been investigated for the first time. An improved understanding of the droplet/ligament effects on turbulence and scalar mixing in the dense spray region is essential to properly model spray dynamics and combustion, and these effects should be taken into account in such a model.

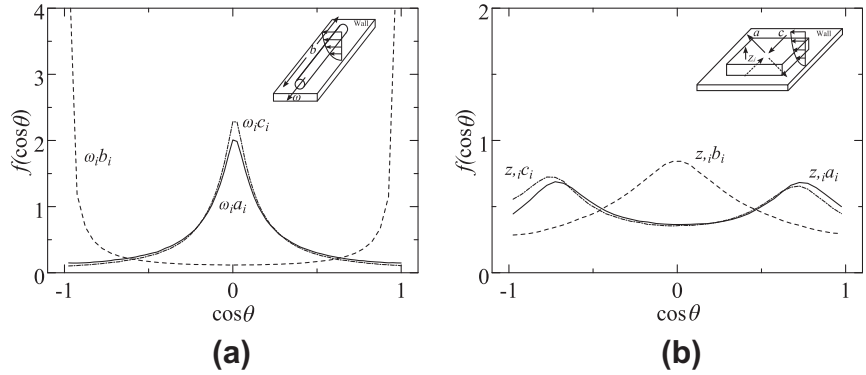

Fig. 7. PDFs of the alignment angles between the principal strain rates and (a) ω_i, (b) z_i in near-droplet regions. (a) Vorticity (b) scalar gradient.

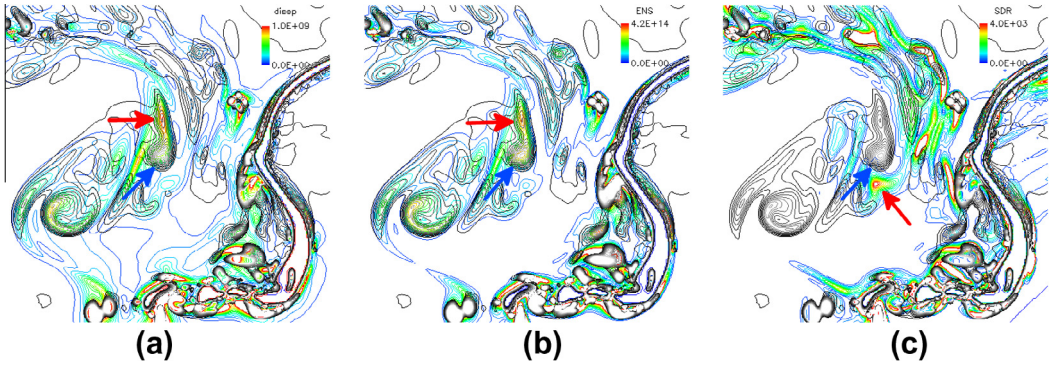

Fig. 8. Close-up view of the instantaneous flow field. (a) Energy dissipation ε ($m^2\,s^{-3}$); (b) enstrophy $\omega_i\omega_i$ (s^{-2}); (c) scalar dissipation Dz_iz_i (s^{-1}).

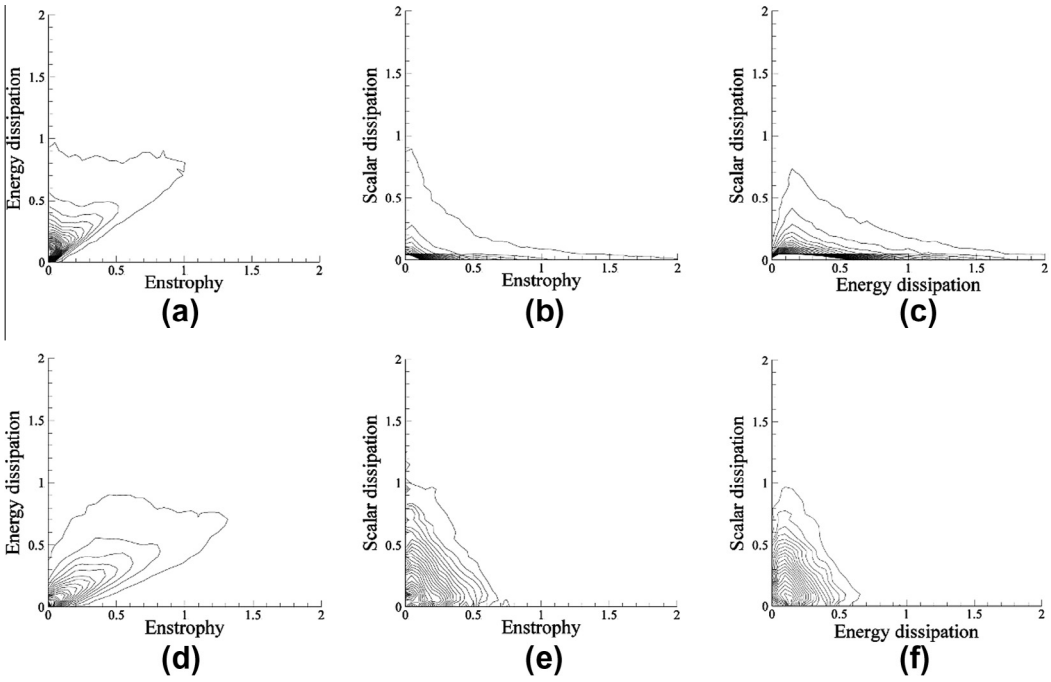

Fig. 9. Joint PDFs in (a–c) the far-surface region and (d–f) the near-surface region.

Acknowledgments

The first author is grateful to Dr. H. Abe for discussions. Financial support from the Engineering and Physical Sciences Research Council (EPSRC) of the United Kingdom under the Grant No. EP/L000199/1 is gratefully acknowledged.

References

[1] M. Linne, *Prog. Energy Combust. Sci.* 39 (2013) 403–440.
[2] M. Gorokhovski, M. Herrmann, *Annu. Rev. Fluid Mech.* 40 (2008) 343–366.
[3] J. Shinjo, A. Umemura, *Int. J. Multiphase Flow* 36 (2010) 513–532.
[4] J. Shinjo, A. Umemura, *Proc. Combust. Inst.* 33 (2011) 2089–2097.
[5] J. Shinjo, A. Umemura, *Int. J. Multiphase Flow* 37 (2011) 1294–1304.
[6] J. Shinjo, A. Umemura, *Proc. Combust. Inst.* 34 (2013) 1553–1560.
[7] G.R. Ruetsch, M.R. Maxey, *Phys. Fluids A* 3 (1991) 1587–1597.
[8] A. Pumir, *Phys. Fluids* 6 (1994) 2118–2132.
[9] K.A. Buch, W.J.A. Dahm, *J. Fluid Mech.* 317 (1996) 21–71.
[10] Wm.T. Ashurst, A.R. Kerstein, R.M. Kerr, C.H. Gibson, *Phys. Fluids* 30 (1987) 2343–2353.
[11] P. Vedula, P.K. Yeung, R.O. Fox, *J. Fluid Mech.* 433 (2001) 29–60.
[12] P.K. Yeung, S.S. Girimaji, S.B. Pope, *Combust. Flame* 79 (1990) 340–365.
[13] H.M. Blackburn, N.N. Mansour, B.J. Cantwell, *J. Fluid Mech.* 310 (1996) 269–292.
[14] H. Abe, R.A. Antonia, H. Kawamura, *J. Fluid Mech.* 627 (2009) 1–32.
[15] S. Elghobashi, G.C. Truesdell, *Phys. Fluids A* 5 (1993) 1790–1801.
[16] A. Ferrante, S. Elghobashi, *Phys. Fluids* 15 (2003) 315–329.
[17] V. Sankaran, S. Menon, *Proc. Combust. Inst.* 29 (2002) 577–584.
[18] T.M. Burton, J.K. Eaton, *J. Fluid Mech.* 545 (2005) 67–111.
[19] F. Lucci, A. Ferrante, S. Elghobashi, *J. Fluid Mech.* 650 (2010) 5–55.
[20] L. Botto, A. Prosperetti, *Phys. Fluids* 24 (2012) 013303.
[21] M. Masoudi, W.A. Sirignano, *Int. J Multiphase Flow* 26 (2000) 1925–1949.
[22] M.R.G. Zoby, S. Navarro-Martinez, A. Kronenburg, A.J. Marquis, *Proc. Combust. Inst.* 33 (2011) 2117–2125.
[23] M. Birouk, I. Gökalp, *Prog. Energy Combust. Sci.* 32 (2006) 408–423.
[24] S. Tanguy, T. Ménard, A. Berlemont, *J. Comput. Phys.* 221 (2007) 837–853.
[25] M.M. Rogers, R.D. Moser, *Phys. Fluids* 6 (1994) 903–923.
[26] M. Olsson, L. Fuchs, *Phys. Fluids* 8 (1996) 2125–2137.
[27] T.A. Johnson, V.C. Patel, *J. Fluid Mech.* 378 (1999) 19–70.
[28] C.H.K. Williamson, *Annu. Rev. Fluid. Mech.* 28 (1996) 477–539.